aerospace

MDPI

Article

A Comparative Study on Harmonic Cancellation in Dual-Generator Power Systems of More-Electric Aircraft

Zhen Huang [1], Chao Wang [1], Yuan Gao [2,*], Hengliang Zhang [3], Zhan Li [4] and Pat Wheeler [5]

[1] School of Information Engineering, Nanchang University, Nanchang 330000, China; zhenhuang@ncu.edu.cn (Z.H.); chaow@email.ncu.edu.cn (C.W.)
[2] School of Engineering, University of Leicester, Leicester LE1 7RH, UK
[3] School of Electrical Engineering, Southeast University, Nanjing 210096, China; zhanghengliang@seu.edu.cn
[4] College of Electrical and Information Engineering, Hunan University, Changsha 410012, China; lizhan@hnu.edu.cn
[5] Department of Electrical and Electronic Engineering, Faculty of Engineering, University of Nottingham, Nottingham NG7 2RD, UK; pat.wheeler@nottingham.ac.uk
* Correspondence: yuan.gao@leicester.ac.uk

Abstract

Switching harmonics generated by power electronic converters have become a critical power quality issue in more-electric aircraft (MEA) dual-generator power systems, and accurate harmonic prediction is essential for effective harmonic cancellation. However, conventional analytical models often suffer from limited prediction accuracy, while data-driven methods are constrained by the scarcity of labeled data under certain operating conditions. This paper presents a method for harmonic prediction and cancellation in the dual-generator power systems of more-electric aircraft. To address the accumulation of switching harmonics on the DC bus, a comparative study is conducted among simplified analytical models, feedforward neural networks, and transfer learning-based models. A harmonic modeling framework and phase shift optimization strategy are established for harmonic cancellation. To overcome data limitations on the high-pressure shaft, transfer learning is employed to transfer knowledge learned from the low-pressure side to the high-pressure side. Results show that data-driven methods outperform traditional models, while transfer learning-based models further improve prediction accuracy and generalization under limited data conditions.

Keywords: dual-generator power system; feedforward neural network; more-electric aircraft; transfer learning

Check for updates

Academic Editor: Kung-Ming Chung

Received: 2 June 2026
Revised: 4 July 2026
Accepted: 6 July 2026
Published: 10 July 2026

Copyright: © 2026 by the authors. Licensee MDPI, Basel, Switzerland. This article is an open access article distributed under the terms and conditions of the Creative Commons Attribution (CC BY) license.

1. Introduction

With the rapid development of electrification technologies and the increasing demand for onboard electrical power, More-Electric Aircraft (MEA) has become an important development direction in the aerospace industry. By replacing traditional hydraulic, pneumatic, and mechanical subsystems with electrical systems, MEA can improve system efficiency, reliability, and environmental performance [1–3]. To satisfy the continuously growing power demand, dual-generator and multi-source electrical architectures have been introduced to simultaneously extract electrical power from both the low-pressure (LP) and high-pressure (HP) shafts of the aircraft engine, thereby improving power capability and operational stability [4,5].

As shown in Figure 1, two generators are respectively driven by the HP and LP shafts of the aircraft engine [6], and each supplies power to the same common DC bus through an

AC-DC converter. As one of the core components of a MEA, the AC-DC converter is mainly used to regulate and convert the AC power output from the generator [7,8]. However, due to the rapid switching structure, switching harmonics and sideband harmonics are inevitably generated during its operation. Due to the difference in shaft speed driving the two generators, the fundamental frequencies of each converter are different from each other. The inconsistency in fundamental frequencies can cause differences in the sideband harmonic frequencies output by the two converters, which poses great difficulties for sideband harmonic cancellation work and will not be discussed in this article. For switch harmonics, their frequency is only determined by the switch frequency and is independent of the fundamental frequency. Therefore, the mismatch between the fundamental frequencies of the two axes does not cause frequency shift of such harmonic components but may instead cause them to continuously accumulate and stack on the DC bus side [9]. Excessive harmonic accumulation may deteriorate power quality, increase capacitor ripple stress, and cause electromagnetic interference, making harmonic suppression a critical issue in MEA power system design [6,7].

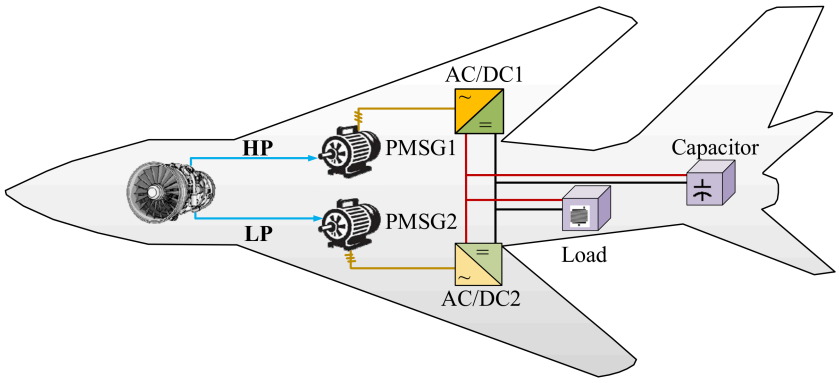

Figure 1. The dual-generator power system of MEA.

Existing studies have mainly focused on analytical harmonic modeling and phase-shift-based harmonic cancellation methods [9,10]. By adjusting the phase angle between the two converters, dominant switching harmonics can be effectively reduced without additional hardware. However, these approaches rely heavily on accurate harmonic models and often exhibit limited adaptability under varying operating conditions and wide speed ranges [9,10]. In particular, simplified analytical models may suffer from reduced prediction accuracy under low-power operating conditions [11].

Recently, neural network (NN) techniques have attracted considerable attention because of their strong nonlinear mapping capability, fast computation, and high prediction accuracy [12]. Previous studies have demonstrated the effectiveness of NN-based methods for harmonic prediction and suppression in MEA and other power electronic systems [13–15]. Nevertheless, the performance of conventional feedforward neural networks (FNN) generally depends on large-scale training datasets, and the associated data collection and training processes can be both time-consuming and costly [16].

In practical aircraft electrical systems, acquiring large-scale, high-quality datasets is costly and challenging, especially on the HP shaft of a dual-generator power system due to its high-speed and high-temperature operating conditions. Furthermore, variations in operating conditions and sensing environments across subsystems can limit the effectiveness of conventional data-driven models, motivating the adoption of knowledge-transfer strategies for cross-domain adaptation [17].

To address the above limitation, transfer learning (TL) provides a promising solution. By reusing knowledge learned from a related source task, TL can reduce the dependence

on large-scale target-domain data while improving model generalization and training efficiency [16,17]. Recent studies have shown the potential of TL in electrical machine design, fault diagnosis, and power electronic applications [18,19]. Since the LP side and HP side generators in dual-generator power systems share similar electrical structures and harmonic generation mechanisms, TL is particularly suitable for transferring knowledge from the LP side to the HP side under data-constrained conditions. However, the effectiveness of TL for harmonic prediction and cancellation in dual-generator power systems has not been systematically investigated, especially in comparison with traditional simplified models and conventional FNN approaches. Its comprehensive advantages and application boundaries still need to be further explored, which is the main motivation for the research performed in this paper.

This paper presents a new solution for the harmonic prediction problem in MEA dual-generator power systems and systematically compares the performance of traditional simplified models, standard NN models, and TL models. With the constructed unified evaluation framework, this paper conducts a multi-dimensional analysis of different methods in terms of prediction accuracy, generalization ability and data requirements. On the basis of the comprehensive evaluation results, phase angle optimization strategies are further integrated to realize effective harmonic cancellation. Through comparative research, this article aims to identify the optimal modeling method and provide a theoretical basis and engineering reference for the design of harmonic prediction and suppression strategies in dual-generator power systems.

The main contributions of this paper are as follows:

1. A harmonic prediction comparison framework is constructed for the MEA dual-generator power system, which quantitatively assesses the merits and demerits of traditional simplified, FNN and TL-based models.
2. A harmonic cancellation strategy combining harmonic prediction and phase shift optimization is developed to suppress DC-bus switching harmonics in dual-generator power systems.
3. The performance of multiple models is comprehensively compared to identify the optimal model under each working condition, and the robustness and feasibility are validated to support follow-up research.

The article structure is organized as follows. Section 2 elaborates on the modeling of DC bus harmonics and the principle of phase shift angle suppression. In Section 3, the FNN and TL methodologies, together with the dataset construction process and model training procedures, are presented. Section 4 provides simulation results and comparative analyses of different modeling approaches in terms of harmonic prediction accuracy and harmonic cancellation performance. Finally, Section 5 summarizes the main conclusions of this study and discusses the potential application value of TL in future aerospace power systems.

2. Principle of Harmonic Modeling and Cancellation

2.1. Harmonic Modeling

The DC bus current i_{dc} is essentially the sum of the output currents from the three-phase branches [9]. Since there is no phase shift among the carrier signals of the three branches and the three-phase currents are shifted by $2\pi/3$, the current components $i_{dc,i,j}$ are zero for all j except when $j = 0, \pm3, \pm6, \ldots$. ($i$ and j denote the harmonic order of the main switching and sideband harmonics of the DC current).

Therefore, harmonic components on the DC bus appear only at the frequencies $f_c, f_c \pm 3f_0$, $f_c \pm 6f_0$, $2f_c$, $2f_c \pm 3f_0$, and $2f_c \pm 6f_0$ (f_c is the switching frequency, and f_0 is the fundamental frequency of the AC side voltage). The spectrum of i_{dc} is shown in

Figure 2. Since the harmonic amplitudes become negligible for $i > 2$ and $j > 6$, their impact on capacitor voltage ripple is minimal and can be ignored in this analysis.

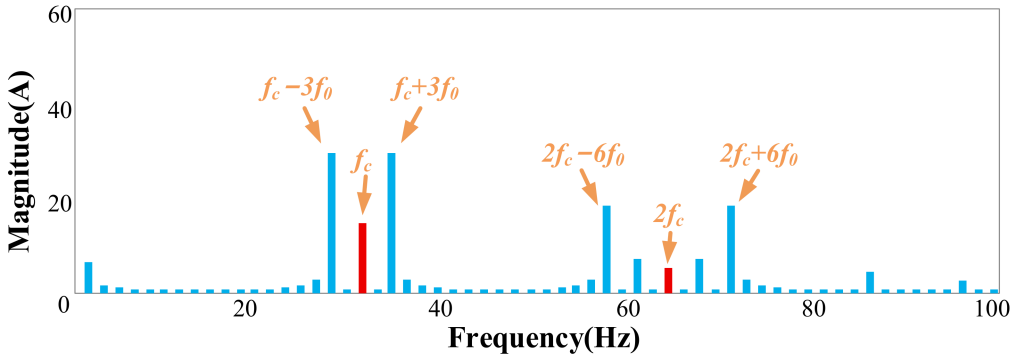

Figure 2. The spectral analysis of DC bus current i_{dc}.

In modeling harmonic amplitudes in power electronics, the Bessel function is used to analyze and calculate them, as defined in Equation (1). Based on this equation, the quantitative magnitude of each harmonic can be quickly obtained.

$$K_{m,n} = \frac{4}{m\pi^2}\left[\begin{array}{l} \frac{\pi}{6}\sin[(q_{m,n}+n)\frac{\pi}{2}]\left\{J_n\left(\frac{3\pi}{4}q_{m,n}M\right)+2\cos\left(\frac{n\pi}{6}\right)J_n\left(\frac{\sqrt{3}\pi}{4}q_{m,n}M\right)\right\} \\ +\frac{1}{n}\sin\left(\frac{q_{m,n}\pi}{2}\right)\cos\left(\frac{n\pi}{2}\right)\sin\left(\frac{n\pi}{6}\right)\left\{J_0\left(\frac{3\pi}{4}q_{m,n}M\right)-J_0\left(\frac{\sqrt{3}\pi}{4}q_{m,n}M\right)\right\} \\ +\sum\limits_{k=1(k\neq -n)}^{\infty}\left[\begin{array}{l}\frac{1}{n+k}\sin\left[(q_{m,n}+k)\frac{\pi}{2}\right]\cos\left[(n+k)\frac{\pi}{2}\right]\sin\left[(n+k)\frac{\pi}{6}\right] \\ \times\left\{J_k\left(\frac{3\pi}{4}q_{m,n}M\right)+2\cos\left((2n+3k)\frac{\pi}{6}\right)J_n\left(\frac{\sqrt{3}\pi}{4}q_{m,n}M\right)\right\}\end{array}\right] \\ +\sum\limits_{k=1(k\neq n)}^{\infty}\left[\begin{array}{l}\frac{1}{n-k}\sin\left[(q_{m,n}+k)\frac{\pi}{2}\right]\cos\left[(n-k)\frac{\pi}{2}\right]\sin\left[(n--k)\frac{\pi}{6}\right] \\ \times\left\{J_k\left(\frac{3\pi}{4}q_{m,n}M\right)+2\cos\left((2n-3k)\frac{\pi}{6}\right)J_n\left(\frac{\sqrt{3}\pi}{4}q_{m,n}M\right)\right\}\end{array}\right] \end{array}\right] \quad (1)$$

where the amplitude of sideband harmonics can be directly represented by the first type Bessel function J_k, and the order k is a non-negative integer. m and n denote the orders of the main harmonic and sideband harmonic in a single-phase leg (e.g., when m and n are 1 and 6, respectively, $K_{m,n}$ represents the magnitude of harmonic components at frequencies $f_c + 6f_0$). The auxiliary coefficient $q_{m,n}$ can be obtained by the following:

$$q_{m,n} = m + n\frac{f_0}{f_c} \quad (2)$$

where K_1 and K_2 are simplified representations of the single-phase harmonic amplitude $K_{m,n}$, as defined by the following two equations:

$$K_1 \approx \frac{3f_cK_{1,-1}}{f_0} \approx -\frac{3f_cK_{1,-1}}{f_0} \quad (3)$$

$$K_2 \approx K_{2,1} \approx K_{2,-1} \quad (4)$$

In the simplified model, M represents the modulation index of the AC-DC converter. Due to the high-speed operation of the permanent magnet synchronous generator (PMSG) in MEA, magnetic flux weakening is necessary. Since the value of M is set to

1.10 ($0.95 \times 2/\sqrt{3}$) under high-speed weak magnetic conditions, and the variation range of K_1 and K_2 is less than $\pm 3\%$, they are subsequently considered constant.

The amplitudes of the first and second switching harmonics ($i_{dc,1,0}$ and $i_{dc,2,0}$) can be derived from the following Equations:

$$i_{dc,1,0}(t) \approx \frac{f_0}{f_c} K_1 \frac{v_q i_d - v_d i_q}{\sqrt{v_d^2 + v_q^2}} \cos\left[2\pi f_c t + \theta_c - \frac{\pi}{2}\right] \tag{5}$$

$$\begin{aligned} i_{dc,2,0}(t) &\approx 3 I_{ac} \cos\alpha K_2 \cos[2 \times (2\pi f_c)t + 2\theta_c] \\ &\approx 3\sqrt{i_d^2 + i_q^2} \cos\alpha K_2 \cos[2 \times (2\pi f_c)t + 2\theta_c] \end{aligned} \tag{6}$$

where the phase angle of the first and second switching harmonics is only determined by the phase angle of the carrier signal (θ_c). By adjusting the switching time of each converter, this component can be actively suppressed. Equation (5) shows that the $i_{dc,1,0}$ depends on the generator-side currents i_d, i_q, voltages v_d, v_q, and the switching frequency f_c, which are all measurable. Moreover, for the first switching harmonic in the dual-generator power system, if the phase shift angle difference between the two channels is 180 degrees, the first switching harmonic can be effectively canceled.

In Equation (6), since cosα is a function of power P and losses are assumed negligible, under known rotational speed conditions, the second switching harmonic can be approximated using the generator-side voltage and current measurements. Moreover, in a dual-generator power system, if the phase shift angle difference between the two channels is 90 degrees, the second switching harmonic can be effectively canceled.

In summary, both the first and second switching harmonics are related to the generator-side parameters and exhibit certain similarities. This provides a theoretical basis for the application of TL.

2.2. Harmonic Cancellation

Due to the need for different phase shift angles to suppress the harmonics of the first and second orders, an optimized compromise solution must be determined. Therefore, total harmonic distortion is introduced here for comprehensive evaluation of the overall harmonic cancellation level. By analyzing the weighted total harmonic of the DC bus capacitor, denoted as the $I_{hf,1,2}$, the impact of the first and second switching harmonics on the capacitor can be quantitatively evaluated. In the MEA dual-generator power system, since the fundamental frequencies on the generator sides differ, only the harmonics at f_c and $2f_c$ can potentially be canceled, i.e.,

$$I_{hf,1,2} = f_c \sqrt{\left(\frac{I_{1f}}{f_c}\right)^2 + \left(\frac{I_{2f}}{2f_c}\right)^2} = \sqrt{I_{1f}^2 + \frac{I_{2f}^2}{4}} \tag{7}$$

where I_{1f} and I_{2f} represent the amplitudes of the first and second switching harmonics, respectively. By calculating the $I_{hf,1,2}$, the effectiveness of harmonic cancellation on the DC bus capacitor can be assessed. A lower $I_{hf,1,2}$ value indicates reduced ripple on the DC bus.

For the first and second switching harmonics, cancellation requires distinct phase angles. Therefore, an optimal compromise must be identified to suppress both harmonics simultaneously. Ref. [9] proposed a phase shift angle suppression strategy. This method achieves concurrent elimination of the first and second switching harmonics by fixing the

carrier phase of one converter and adjusting that of the other. The implementation process is illustrated in Figure 3, and the phase shift angle ($\Delta\theta_c$) can be obtained by the following:

$$\Delta\theta_c = \begin{cases} \cos^{-1}\left(-\frac{I_1^{\{1\}} I_1^{\{2\}}}{I_2^{\{1\}} I_2^{\{2\}}}\right), & \frac{I_1^{\{1\}} I_1^{\{2\}}}{I_2^{\{1\}} I_2^{\{2\}}} < 1 \\ \pi, & \frac{I_1^{\{1\}} I_1^{\{2\}}}{I_2^{\{1\}} I_2^{\{2\}}} \geq 1 \end{cases} \tag{8}$$

By adjusting the phase shift angle, the $I_{hf,1,2}$ can be effectively reduced.

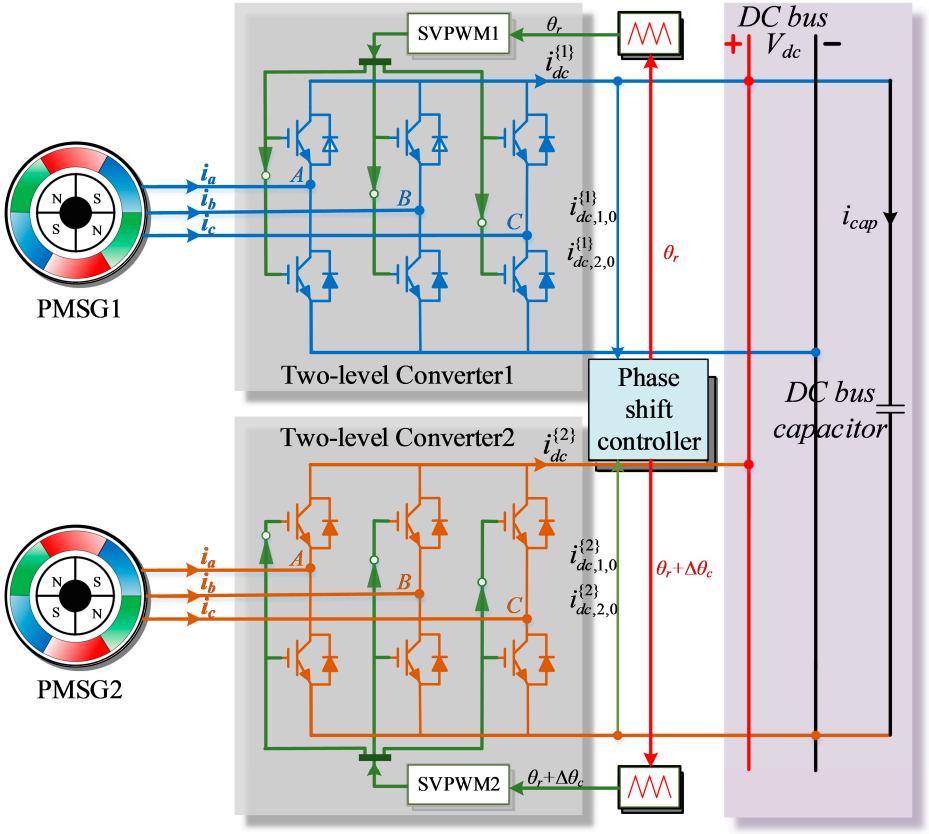

Figure 3. The phase angle control principle of a dual-generator power system.

3. FNN and TL Methods

3.1. Data Collection

The data collection steps involved constructing datasets for the source domain (the LP side) and the target domain (the HP side). The source domain dataset was obtained from the dual-generator power system model established in MATLAB/Simulink 2024a. By simulating various operating conditions, a comprehensive dataset was generated to ensure sufficient coverage and diversity. The input features of the five-input model included the current and voltage i_d, i_q, v_d, v_q of the dq axis, as well as the rotational speed n. The input features of the four-input model included the stator current and voltage i_{dq}, v_{dq}, rotational speed n, and power P. In addition, the corresponding outputs were defined as the amplitudes of the first and second switching harmonics. The target domain consisted of similar input features and harmonic amplitude data, which came from the HP end with higher speed and power, so the sample size was limited.

Figure 4 illustrates the distribution of voltage and current operating points on the generator side in the dq reference frame. Each point represents a sampled operating condition obtained by applying a fixed angular increment. As the sampling angle increases

progressively over the full range, the resulting voltage and current points form concentric circular patterns in the polar coordinate representation. The outermost points, referred to as boundary state points, correspond to the maximum allowable voltage and current levels, thereby defining the safe operating limits of the generator.

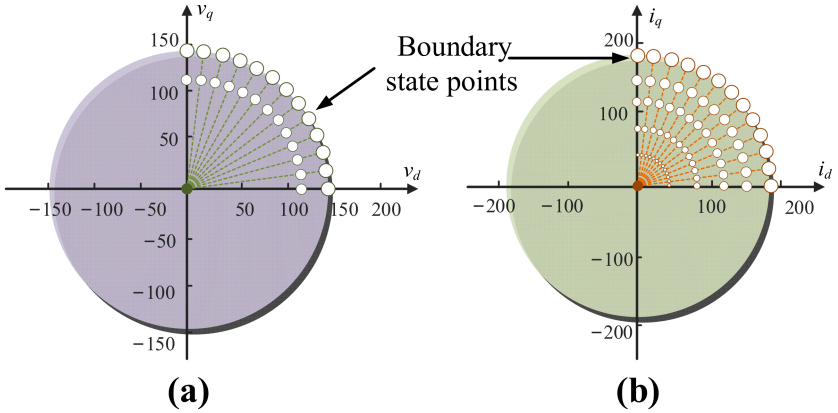

Figure 4. Distribution of dq axis voltage and current state points. (**a**) Stator voltage (v_d, v_q) polar coordinate distribution. (**b**) Stator current (i_d, i_q) polar coordinate distribution.

During the data collection process, the rotational speed gradually increased from 6 *k*rpm to 32 *k*rpm. At each speed level, voltage and current samples were collected using the same angular increment strategy. For every sampled state point, the corresponding dq-axis voltages, currents, and rotational speed were recorded and used as input variables for the MEA dual-generator power system model. Subsequently, under different simulated load conditions and operating speeds, the associated harmonic amplitudes were obtained. Following this procedure, the complete dataset for model training was constructed.

3.2. FNN Modeling Method

To predict the switching harmonic amplitudes of the dual-generator power system, an FNN was adopted to establish nonlinear mapping between the operating variables and harmonic responses. Compared with simplified models, the FNN directly learns this relationship from data without requiring an explicit mathematical description of the system [20].

An FNN consists of an input layer, one or more hidden layers, and an output layer. Each neuron performs a weighted summation followed by a nonlinear activation function, which can be expressed as

$$y = \sigma\left(\sum_{i=1}^{n} \omega_i x_i + b\right) \tag{9}$$

where ω_i denotes the network weights, b is the bias term, and σ represents the activation function. The nonlinear activation enables the network to approximate the complex relationship between the operating conditions and harmonic amplitudes.

Based on the dataset constructed above, separate FNN models were trained for the LP and HP sides using 9060 and 5436 samples, respectively. The network adopted three hidden layers, and the model parameters were optimized through backpropagation by minimizing the prediction error. After training, the FNN provided the predicted amplitudes of the first and second switching harmonics, which were subsequently used for the phase shift optimization.

3.3. TL Method

Despite the strong capability of FNNs in modeling complex nonlinear systems, their performance typically relies on large-scale datasets, and the associated training process often incurs considerable computational and time costs. To improve prediction performance under limited HP side data, a TL framework was developed based on the FNN model. As illustrated in Figure 5, the TL framework consists of two stages: source-domain pre-training and target-domain fine-tuning.

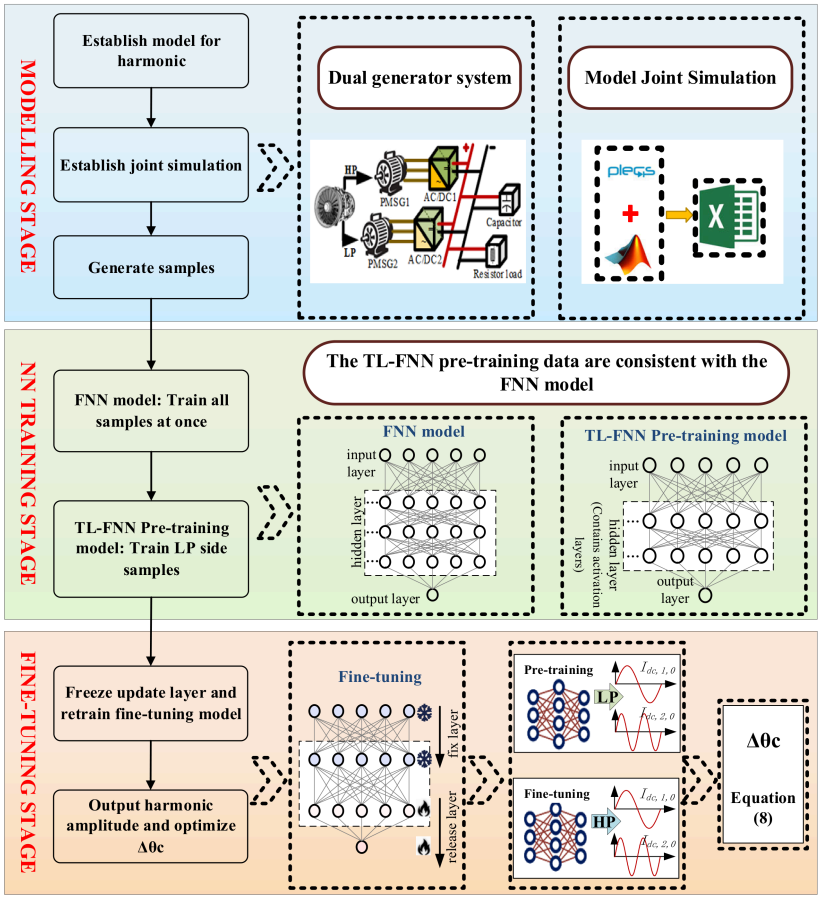

Figure 5. FNN and TL model training process framework.

3.3.1. Model Pre-Training

Based on the collected dataset in the previous section, a TL model was established. The network consists of an input layer, two hidden layers, and an output layer. In this structure, the input signals are propagated layer by layer through weighted connections and bias terms, where each neuron computes a weighted summation, followed by a nonlinear activation function to determine its output.

In the application of this paper, the two hidden layers contained 128 and 16 neurons, respectively, both employing the rectified unit (ReLU) as the activation function. The introduction of nonlinear activation enables the network to effectively capture complex relationships between electrical variables, thereby enhancing its capability to model the nonlinear characteristics of DC bus harmonic behavior.

The selection of network depth and neuron configuration was determined through iterative evaluation and comparative analysis. Initially, the number of neurons in the first hidden layer was progressively increased, and the corresponding root mean square error (RMSE) was monitored to assess model performance. An elbow point was identified to balance accuracy and computational complexity, which determined the appropriate

width of the first layer. While a single hidden layer with a large number of neurons may lead to overfitting due to excessive model capacity, the adoption of a two-layer structure with a gradually reduced number of neurons introduces an implicit regularization effect. This "wide-to-narrow" architecture improves generalization by compressing feature representations across layers. Following a similar procedure, the number of neurons in the second hidden layer was determined. The final network configuration represents a compromise between prediction accuracy and training efficiency. The model training framework shown in Figure 5 also includes this process.

During training, a two-stage early stopping strategy was adopted to prevent overfitting. First, 20 pilot training runs with different random initializations were performed to estimate the expected performance threshold based on the minimum average validation error. During formal training, the test RMSE was evaluated every 50 iterations. Training was terminated if the RMSE failed to improve by more than 0.1% over six consecutive evaluations, even if the predefined threshold had not been reached. This strategy effectively prevented unnecessary training while maintaining good generalization performance.

In the pre-training stage, the FNN was trained using data from the LP side to learn the underlying nonlinear mapping between input variables and harmonic amplitudes. The resulting model serves as a well-initialized source network, facilitating efficient knowledge transfer in subsequent stages.

3.3.2. Model Fine-Tuning

After completing the pre-training stage in the source domain, the TL framework was applied to adapt the model to the target domain (the HP side). Owing to the strong similarity between the source and target systems in terms of physical configuration and harmonic generation mechanisms, both domains share an identical input feature space, including i_d, i_q, v_d, v_q and n. The primary difference lies in the variation of harmonic amplitude distributions caused by distinct operating conditions.

Based on this observation, the feature extraction layers of the pre-training model comprising the input layer and the first hidden layer along with its activation function were retained and frozen during the transfer process. By preserving these layers, the model maintained the generalized feature representations learned from the source domain, effectively mitigating the risk of overfitting when only a limited amount of target domain data is available.

Subsequently, the higher-level layers of the original network, including the second hidden layer and the output layer, were replaced with newly initialized layers tailored to the target task. These newly introduced layers were specifically designed to capture the harmonic characteristics of the HP side. Although the internal parameters differed, the overall network depth remained consistent with that of the pre-training model. During the fine-tuning stage, only the newly added layers were updated, while the frozen layers remained unchanged. Backpropagation was therefore confined to these trainable components, enabling the model to efficiently adapt to the target domain without disrupting the previously learned representations.

This transfer strategy preserved the transferable knowledge learned from the source domain while enabling efficient adaptation to the harmonic distribution in the target domain. By reusing the learned feature representations rather than training a new model from scratch, it reduced the dependence on large target-domain datasets and improved prediction accuracy and generalization under small-sample conditions. Finally, the fine-tuned models were employed to predict the amplitudes of the first and second switching harmonics, respectively. Based on these predictions, the $I_{hf,1,2}$ was calculated using (7) to quantitatively evaluate the combined effect of the dominant harmonic com-

ponents. Furthermore, the phase shift angle was determined according to (8), enabling dynamic adjustment of the phase difference between the two rectifiers to effectively suppress overall harmonic levels.

4. Results and Discussion

A simulation study was undertaken using MATLAB/Simulink 2024a and PLECS 4.9.5 software to verify the performance of the proposed model and harmonic suppression. Table 1 presents the relationship between the basic control parameters and the output power of a single converter. The PMSG used was a six-pole PMSG structure. The switching frequency of the two converters was the same, both at 32 *k*Hz. This design was based on the requirement of a carrier-to-fundamental frequency ratio of 20:1 at maximum speed (32 *k*rpm, 1600 Hz).

Table 1. DC bus parameters for dual-generator power system.

Category	Parameters	Values
PMSG	Steady state rotor parameters	20 *k*rpm & 30 *k*rpm
	Switching frequency (f_c)	32 *k*Hz
	Maximum modulation index (M)	$1.04(0.9 \times 2/\sqrt{3})$
	Current controller bandwidth	1000 Hz
DC bus	DC bus capacitance	400 *u*F
	Load power	20 kW to 80 kW

4.1. Comparison of Model Prediction Accuracy Performance

To evaluate the performance of different modeling methods in the harmonic prediction task of the MEA dual-generator power system, this paper mainly selected RMSE as the evaluation index to compare and analyze the performance of seven models in predicting first and second switching harmonics. The methods considered include: 5-in-1-output FNN, traditional simplified model, subtraction corrected FNN model, 5-in-1-output TL, 5-in-2-output TL, 4-in-1-output TL, and 4-in-1-output FNN model. The predictive performance results of each model are shown in Table 2.

Table 2. Comparison of performance indicators of various methods.

Index	$I_{dc,1,0}$_RMSE	$I_{dc,2,0}$_RMSE	$I_{dc,1,0}$_RSE	$I_{dc,2,0}$_RSE	Time
5-in-1-output FNN	7.19×10^{-4}	5.48×10^{-3}	4.49×10^{-6}	4.21×10^{-7}	199 s
Simplified model	1.26×10^{-2}	4.49×10^{-1}	2.36×10^{-5}	1.46×10^{-4}	/
Subtraction corrected FNN	7.24×10^{-4}	6.38×10^{-4}	4.56×10^{-6}	5.71×10^{-7}	158 s
5-in-1-output TL	3.58×10^{-4}	2.58×10^{-4}	2.31×10^{-6}	1.08×10^{-7}	23 s
5-in-2-output TL	1.74×10^{-1}	3.28×10^{-1}	5.32×10^{-4}	2.83×10^{-4}	107 s
4-in-1-output TL	$\mathbf{3.20 \times 10^{-4}}$	$\mathbf{2.18 \times 10^{-4}}$	$\mathbf{2.06 \times 10^{-6}}$	$\mathbf{9.13 \times 10^{-8}}$	**21 s**
4-in-1-output FNN	6.35×10^{-2}	6.41×10^{-2}	2.80×10^{-4}	1.71×10^{-5}	173 s

RMSE was used to measure the deviation between the predicted values and the true values of a model, and its definition is as follows:

$$RMSE = \sqrt{\frac{1}{N}\sum_{i=1}^{N}(y_i - q_i)^2} \tag{10}$$

where y_i is the true value, q_i is the predicted value, and N is the sample size. The smaller the RMSE, the higher the prediction accuracy of the model.

Furthermore, after introducing TL, the overall performance of each TL model was generally better than that of the corresponding traditional FNN model. This indicates that

TL can effectively improve the predictive ability of the model on the target task, especially in dual-generator power systems with similar LP and HP axes. This is mainly due to its implementation of knowledge transfer between similar tasks, thereby improving the performance of the model under data-constrained conditions. Finally, in comparing TL models with different structures, it can be found that the 4-in-1-output TL model performed the best overall. Compared with the 5-in-1-output TL, this indicates that reducing and optimizing input features can better capture the intrinsic correlations between different harmonic components and improve the overall modeling ability of the model.

Although the 5-in-1-output TL model has a high input dimension, it still maintains excellent performance, which also reflects the robustness of TL in the case of insufficient features.

Interestingly, the TL model with 5-in-1-output performed better than the corresponding TL model with 5-in-2-outputs. This can be attributed to multiple factors. Firstly, the coupling strength between the output features, namely the first and second switching harmonics, is insufficient to benefit from feature sharing, and mandatory unified training may lead to a decrease in accuracy. Secondly, a multi-output structure may cause negative transfer, where the learning of a certain harmonic component can interfere with other components. In addition, in the case of limited data, the increased complexity of multi-output models makes them more difficult to train effectively. Therefore, the 5-in-1-output TL model achieved relatively better overall prediction performance.

Based on the prediction results of the first and second switching harmonics, the 4-in-1-output TL demonstrated the best predictive performance under both evaluation metrics, followed by the 5-in-1-output TL. In contrast, the simplified model and several conventional FNN structures showed relatively larger prediction errors. The next section further evaluates the effectiveness of each model in harmonic cancellation.

4.2. Comparison of Harmonic Cancellation Performance Under Symmetric Allocation

After obtaining the harmonic prediction results of each model, this section further evaluates the performance of different models in actual harmonic cancellation tasks based on phase angle optimization strategies. Unlike the previous section, which only focused on prediction accuracy, this section focuses on analyzing the actual harmonic elimination effects of various models on the DC bus side.

Figures 6 and 7 present the DC bus currents of the two converters ($I_{dc}^{\{1\}}$ and $I_{dc}^{\{2\}}$), along with the harmonic spectra of the DC bus capacitor current I_{cap}. An experiment was conducted under a symmetrical power allocation ratio of 1:1. The results were obtained for each models under the no-cancellation and phase-shift-angle cancellation conditions when the load power was 20 kW and 80 kW. For the harmonic cancellation results of each model, the first and second switching harmonics were obtained by FFT analysis of the I_{cap}, and then the $I_{hf,1,2}$ of the DC bus was then calculated according to Equation (7) to comprehensively and holistically quantify the magnitude of the total harmonic on the DC bus. From the results, it can be seen that each model had a specific harmonic cancellation effect compared to no harmonic cancellation.

Table 3 shows the $I_{hf,1,2}$ after harmonic cancellation using seven methods at 40 kW and 60 kW, respectively, and summarizes the results at 20 kW and 80 kW. According to the experimental results, it can be seen that the harmonic cancellation performance of each method is ranked from best to worst in the full power range as follows: 4-in-1-output TL, 5-in-1-output TL, subtraction-corrected FNN, 5-in-1-output FNN, simplified model, 4-in-1-output FNN, and 5-in-2-output TL. This reflects the convergence of harmonic cancellation for different models under different load powers.

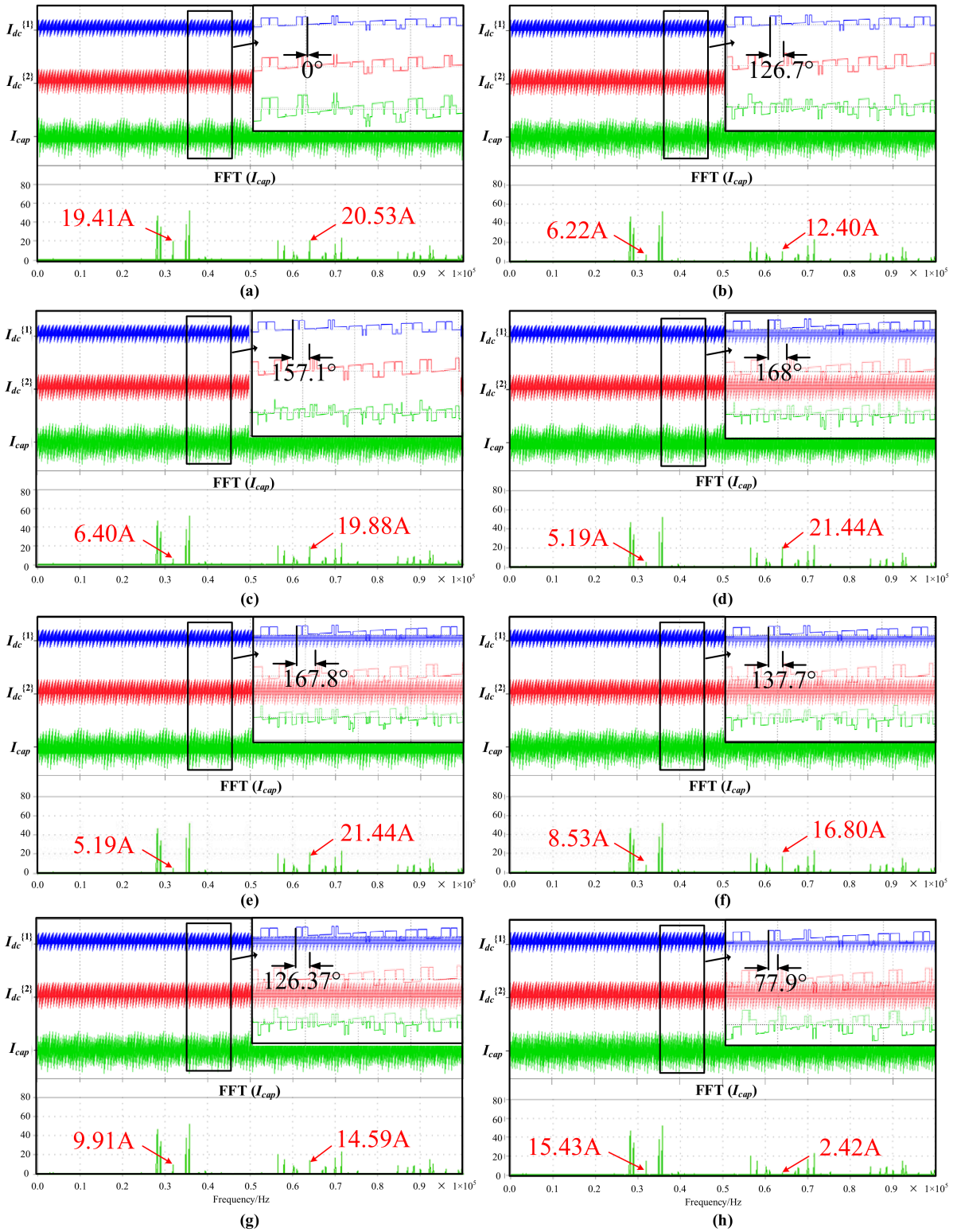

Figure 6. Comparison of harmonic cancellation among various models under 20 kW and 1:1 conditions: (**a**) no harmonic cancellation; (**b**) 4-in-1-output TL; (**c**) 5-in-1-output TL; (**d**) subtraction-corrected FNN; (**e**) 5-in-1-output FNN; (**f**) simplified model; (**g**) 4-in-1-output FNN; (**h**) 5-in-2-output TL.

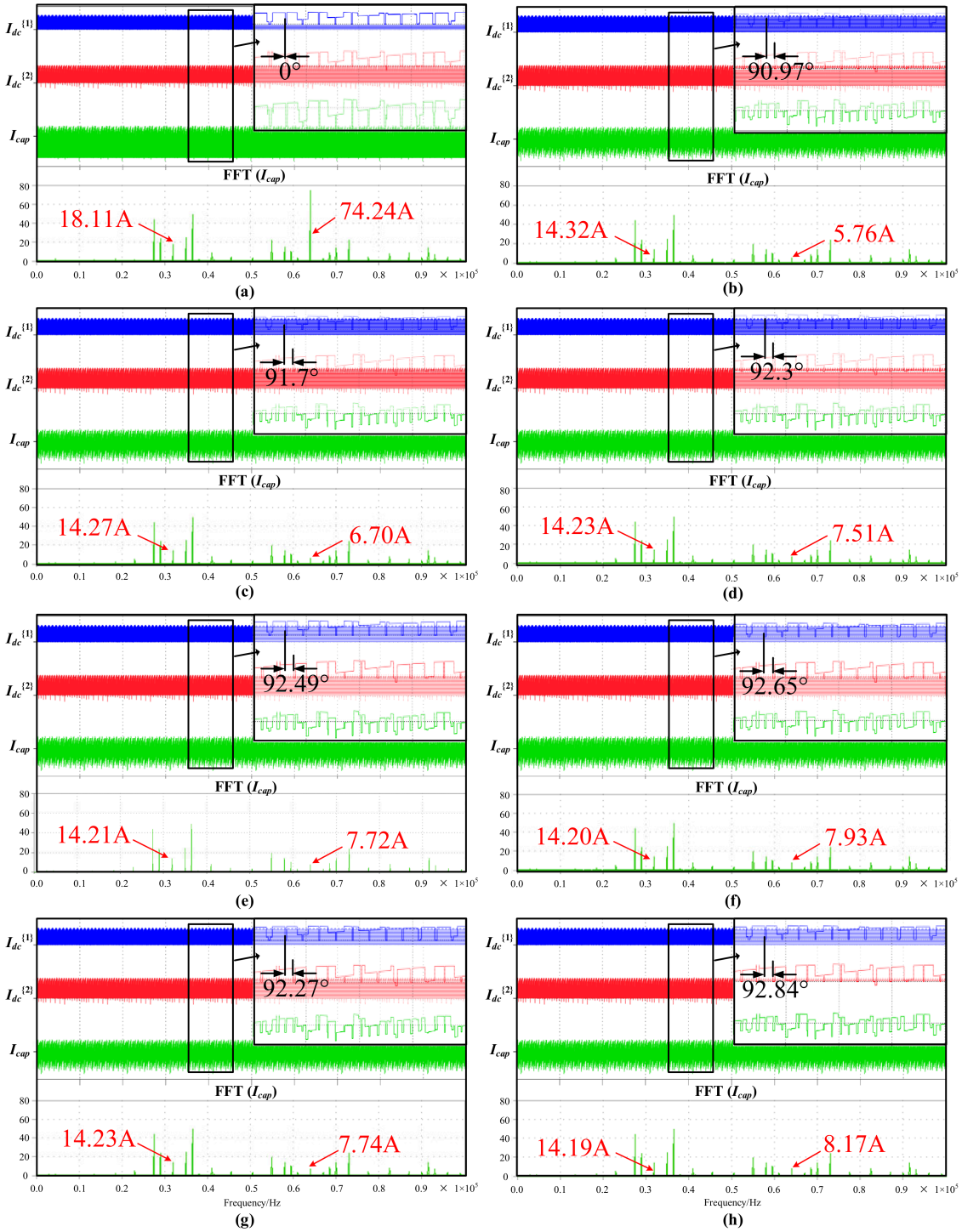

Figure 7. Comparison of harmonic cancellation among various models under 80 kW and 1:1 conditions: (**a**) no harmonic cancellation; (**b**) 4-in-1-output TL; (**c**) 5-in-1-output TL; (**d**) subtraction-corrected FNN; (**e**) 5-in-1-output FNN; (**f**) simplified model; (**g**) 4-in-1-output FNN; (**h**) 5-in-2-output TL.

Among all methods, the 4-in-1-output TL achieved the lowest $I_{hf,1,2}$ values, reaching 8.78 A at 20 kW and 14.61 A at 80 kW. The 5-in-1-output TL provided the second best cancellation performance, while the 5-in-2-output TL exhibited the weakest suppression capability.

Overall, the TL-based models achieved lower residual harmonic levels than the conventional FNN and simplified models across both operating conditions.

Table 3. The $I_{hf,\ 1,2}$ of each method from 20 to 80 kW.

$I_{hf,1,2}$	20 kW	40 kW	60 kW	80 kW
5-in-1-output FNN	11.91 A	18.15 A	16.86 A	14.72 A
Simplified model	11.97 A	18.26 A	16.93 A	14.74 A
Subtraction corrected FNN	11.91 A	18.10 A	16.85 A	14.71 A
5-in-1-output TL	11.82 A	17.99 A	16.84 A	14.66 A
5-in-2-output TL	15.47 A	21.75 A	17.06 A	14.76 A
4-in-1-output TL	**8.78 A**	**17.93 A**	**16.80 A**	**14.61 A**
4-in-1-output FNN	12.30 A	18.51 A	16.97 A	14.75 A

4.3. The Performance Under Asymmetric Allocation and Parameter Mismatch

In the maximum take-off and climb mode of MEA, the HP side must provide greater power than the LP side to prevent overspeed and potential instability issues [21]. Under this constraint, the dual-generator power system will operate in an asymmetric distribution mode. In order to verify the harmonic cancellation effect of the transient process mentioned above, four representative models (4-in-1-output TL, subtraction-corrected FNN, 5-in-1-output FNN, and the simplified model) were selected from the previous section. Based on the engineering background mentioned above, asymmetric verification was conducted under the conditions of maintaining load power at 20 kW and 80 kW. The power allocation ratio was set to 0.8:1. The results are shown in Figures 8 and 9.

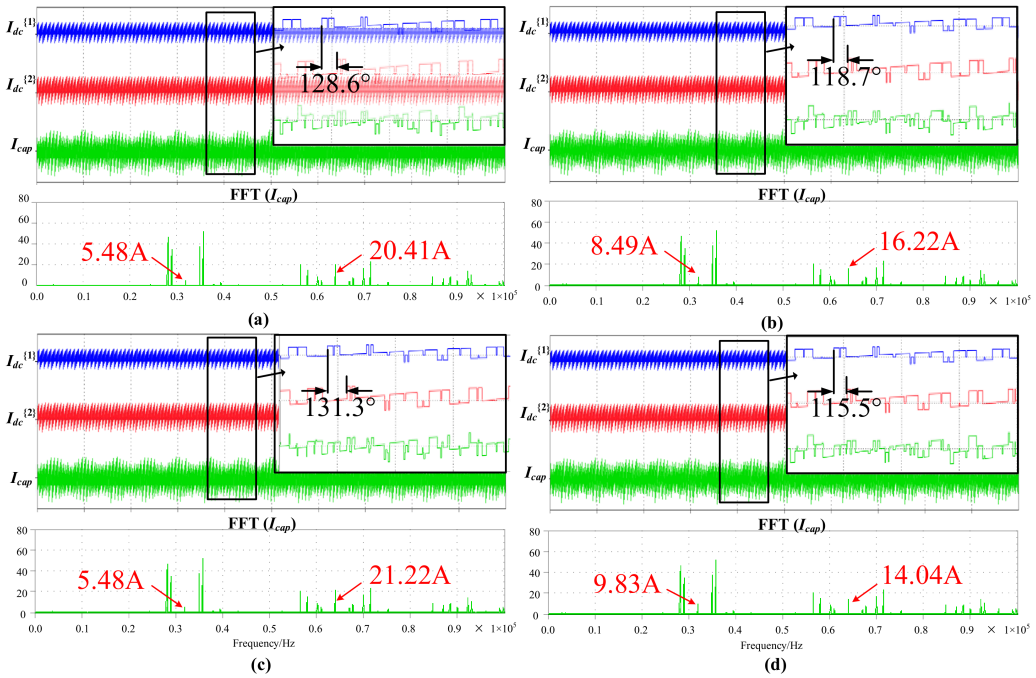

Figure 8. Comparison of harmonic cancellation among various models under 20 kW and 0.8:1 conditions: (**a**) 4-in-1-output TL; (**b**) subtraction-corrected FNN; (**c**) 5-in-1-output FNN; (**d**) simplified model.

In addition, in actual dual-generator power systems, the DC bus capacitance also has a significant impact on the system's dynamic and harmonic characteristics. Therefore, this parameter was also chosen as a representative for robustness evaluation. By reducing the capacitance from its nominal value of 200 μF to 150 μF, the thermal effects and parameter degradation caused by device aging were experimentally simulated at load powers of 20 kW and 80 kW, as shown in Figures 10 and 11.

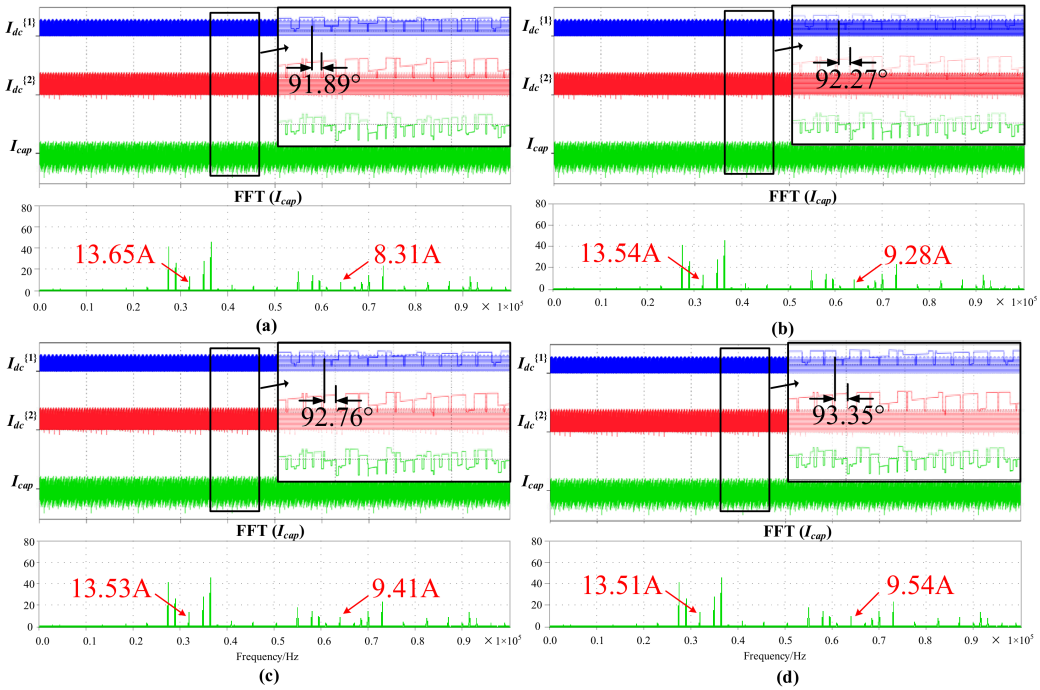

Figure 9. Comparison of harmonic cancellation among various models under 80 kW and 0.8:1 conditions: (**a**) 4-in-1-output TL; (**b**) subtraction-corrected FNN; (**c**) 5-in-1-output FNN; (**d**) simplified model.

The $I_{hf,1,2}$ values in Figures 8–11 are summarized in Table 4. Under asymmetric power distribution, the second switching harmonic becomes dominate. When the power allocation ratio was 0.8:1, all four models had harmonic cancellation effects. Similarly, when the above parameter mismatch occurred, all four models effectively suppressed the first and second switching harmonics while reducing $I_{hf,1,2}$. In addition, the $I_{hf,1,2}$ values of the 4-in-1-output TL model were the lowest compared to the other three models under the two conditions, and the performance ranking of the four models still follows the previous description. This indicates that the model does not strictly rely on nominal parameters and exhibits good robustness even under actual parameter deviations. In summary, these results demonstrate the harmonic elimination effect of each model under asymmetric power allocation ratios, fully demonstrating their excellent robustness.

Table 4. Harmonic cancellation performance of models under asymmetric allocation and parameter mismatch.

Nonideal Conditions	Cancellation Method (Phase Shift Angle)	$I_{hf,1,2}$ at 20 kW	$I_{hf,1,2}$ at 80 kW
0.8:1 power ratio	**4-in-1-output TL**	**11.58 A**	**14.27 A**
	Subtraction corrected FNN	11.73 A	14.31 A
	5-in-1-output FNN	11.94 A	14.32 A
	Simplified model	12.08 A	14.33 A
150 μF DC bus capacitance	**4-in-1-output TL**	**11.72 A**	**14.65 A**
	Subtraction corrected FNN	11.98 A	14.76 A
	5-in-1-output FNN	12.09 A	14.77 A
	Simplified model	12.30 A	14.79 A

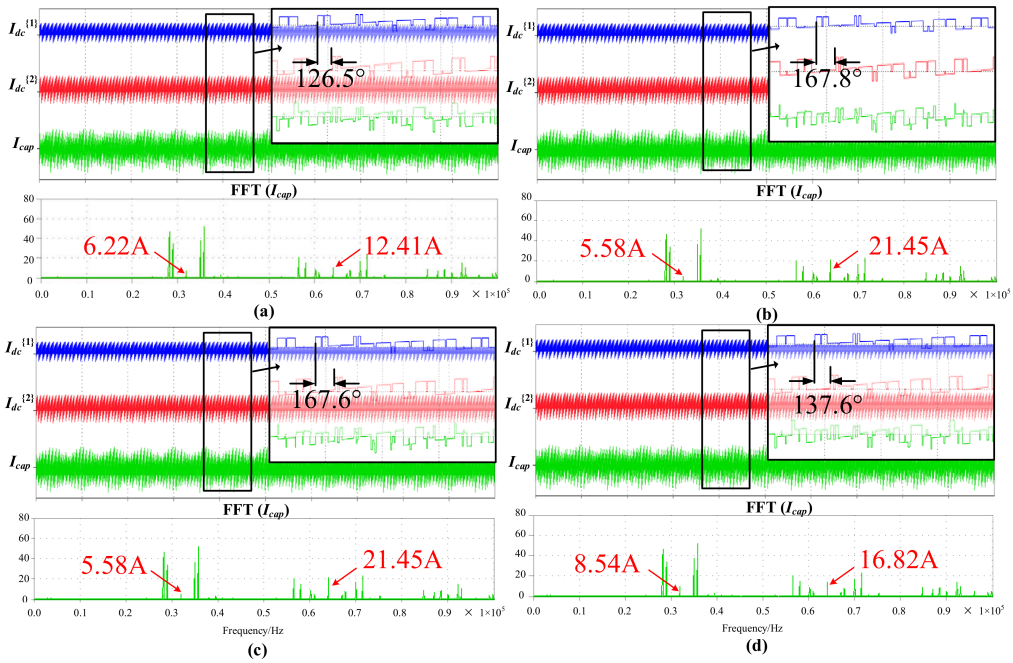

Figure 10. Comparison of harmonic cancellation among various models under a 20 kW parameter mismatch: (**a**) 4-in-1-output TL; (**b**) subtraction-corrected FNN; (**c**) 5-in-1-output FNN; (**d**) simplified model.

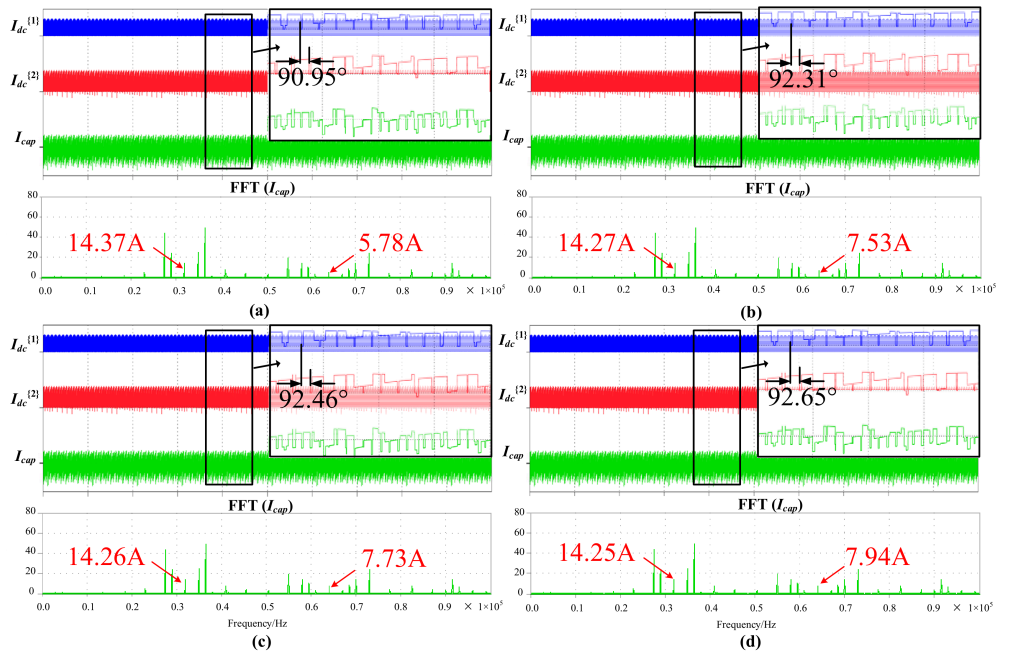

Figure 11. Comparison of harmonic cancellation among various models under a 80 kW parameter mismatch: (**a**) 4-in-1-output TL; (**b**) subtraction-corrected FNN; (**c**) 5-in-1-output FNN; (**d**) simplified model.

4.4. Discussion

From the overall results, TL models still dominate in harmonic cancellation tasks. Among them, the 4-in-1-output TL model achieved the best suppression effect, and $I_{hf,1,2}$ significantly reduced compared to other methods. Based on the overall trend, this ranking has strong consistency with the RMSE ranking of the first and second switching harmonics in the previous section. Specifically, both 4-in-1-output TL and 5-in-1-output TL exhibited lower RMSE in both types of harmonic prediction, corresponding to optimal and sub-

optimal performance in harmonic cancellation results. This indicates that the accuracy of harmonic prediction remains a key factor affecting the effectiveness of harmonic cancellation, and high-precision models can provide more accurate inputs for phase angle optimization, thereby achieving more effective harmonic elimination.

In addition, the harmonic cancellation results exhibit different distribution characteristics at different operating power levels. Taking the symmetrical power allocation ratio as an example, as shown in Figure 12 and Table 3, the 20 kW condition exhibits a wide $I_{hf,1,2}$ distribution among different models, with $I_{hf,1,2}$ values ranging from 8.78 A to 15.47 A, indicating high sensitivity of harmonic cancellation performance to model selection under low-power operation. In contrast, as the load power increased to 60 kW and 80 kW, the output range quickly converged to within 0.3 A, indicating that the outputs of different models are highly stable under high-power conditions. Although the absolute differences between models were small under high-power conditions, the relative ranking overall remained consistent with the previously observed accuracy of harmonic prediction. One possible reason is that under high-power conditions, the amplitude of the second switching harmonic dominates, and the harmonic suppression of each model focuses on the second switching harmonic as the core control objective, with a corresponding phase shift angle close to 90°. Under this operating condition, the characteristic changes of the main harmonic of the DC bus are smoother. This phenomenon implies that increasing operating power tends to reduce the sensitivity of total harmonic cancellation performance to modeling differences, whereas model selection plays a more critical role under lower-power operating conditions.

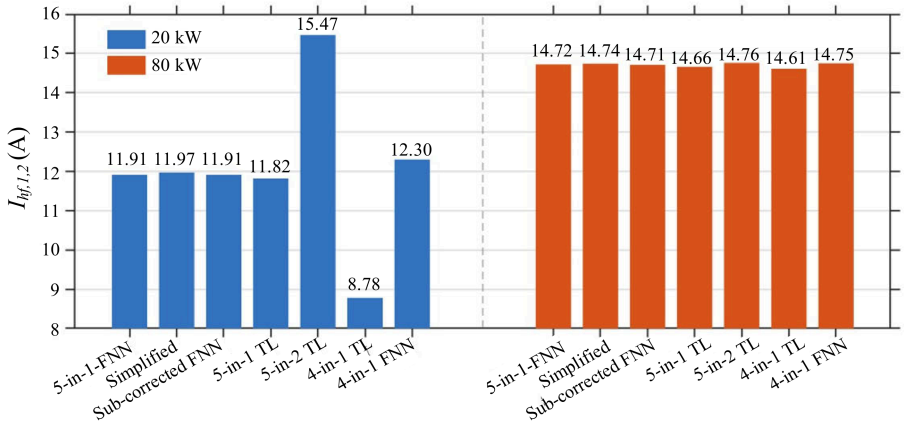

Figure 12. Comparison of harmonic suppression performance among various models.

However, in comparing different models, it can be found that there is not complete one-to-one correspondence between the total harmonic cancellation effect and the accuracy of single harmonic prediction. For example, in first switching harmonic prediction, the 5-in-1-output FNN model outperforms the subtraction corrected FNN model, while in second switching harmonic prediction, the opposite is true. Ultimately, in total harmonic cancellation results, the subtraction-corrected FNN model outperformed the 5-in-1-output FNN model. This phenomenon indicates that the total harmonic level is determined by the superposition of multiple harmonics, and the errors of the model on different harmonic components will also affect the final suppression effect.

In contrast, the subtraction-corrected FNN model outperformed the pure FNN models (5-in-1-output FNN and 4-in-1-output FNN) in terms of suppression performance, indicating that introducing error compensation on the basis of traditional models can improve the harmonic cancellation effect to a certain extent. However, due to its inherent reliance on simplified models, its performance improvement was limited and remained inferior to that of TL. In addition, the performance of the traditional simplified models was at a

moderate level, and their inhibitory effect was weaker than that of the TL models and correction models. This is mainly due to the relatively large harmonic prediction error, which results in the optimized phase angle deviating from the optimal value, thereby reducing the harmonic cancellation efficiency.

To further summarize the characteristics of different modeling approaches, Table 5 presents a qualitative comparison of the investigated methods in terms of prediction accuracy, harmonic cancellation capability, computational efficiency, and model complexity. Rather than focusing solely on numerical performance, this comparison highlights the inherent strengths and limitations of each approach from both modeling and engineering application perspectives.

Table 5. Qualitative comparison of different models.

Models	Accuracy	Harmonic Cancellation	Training Times	Model Complexity
5-in-1-output FNN	√√√	√√√	199 s	√√
Simplified model	√√	√√	/	√√√√
Subtraction-corrected FNN	√√√	√√√	158 s	√√
5-in-1-output TL	√√√√	√√√√	23 s	√√√
5-in-2-output TL	√	√	107 s	√√√
4-in-1-output TL	√√√√	√√√√	**21 s**	√√
4-in-1-output FNN	√√	√√	173 s	√

Rated from best (√√√√) to worst (√).

From an engineering application perspective, simplified models are suitable for scenarios that require high interpretability and negligible training costs, but their prediction accuracy is limited by the established mathematical models. Under the condition of sufficient training data, traditional FNN models have excellent nonlinear fitting modeling capabilities, making them the preferred choice in scenarios with significant differences in task features. However, for similar tasks with similar features, traditional FNN models have the drawbacks of long training cycles and large data requirements, which greatly weaken their application value in data constrained scenarios. In contrast, TL-based models are more suitable for scenarios with limited target-domain data and similar tasks, such as the HP shaft considered in this study. However, their performance relies on sufficient similarity between the source and target domains, and significant differences in operating characteristics may reduce the effectiveness of knowledge transfer. Therefore, model selection should be made by balancing prediction accuracy, data availability, and practical deployment requirements.

Overall, the performance of harmonic cancellation depends crucially on the overall prediction accuracy of the model. However, it is also closely related to the errors of the model at key frequency points and the complexity of the model structure. The TL method demonstrated the best overall performance in this study by enhancing modeling ability under data-constrained conditions. Among them, the 4-in-1-output TL model achieved the optimal balance between accuracy and robustness, verifying its reliability and application value.

5. Conclusions

This paper presents a comparative study on harmonic prediction and cancellation in MEA dual-generator power systems. Results show that traditional models have limited accuracy, while FNN improves nonlinear modeling capability but relies on large datasets. TL effectively reduces data dependency and enhances generalization by leveraging similarities between LP and HP shafts. Among all methods, the 4-in-1-output TL achieved the best balance between accuracy and robustness, leading to superior harmonic suppression

performance. Under symmetrical power allocation ratio, the $I_{hf,1,2}$ decreased to 8.78 A at 20 kW and 14.61 A at 80 kW. In addition, it requires the shortest training time and has the lowest training cost compared to other models. Under the conditions of asymmetric power allocation ratio and parameter mismatch, the robustness of the model was also verified. The study demonstrates the effectiveness of TL for data-constrained aerospace power systems and provides guidance for harmonic modeling and control design.

Future work will proceed in two complementary directions to further strengthen the proposed framework. First, future research will quantify the system-level gain of harmonic cancellation, including the weight reduction of DC link capacitors, the impact on fuel consumption, and the extension of capacitor lifespan. Second, future work will explore the integration of more advanced online intelligent learning algorithms, such as the fixed-time reinforcement learning fault-tolerant control strategy recently proposed by Wang et al. [22], to enhance the robustness of the system under fault transients. Ultimately, through the above system-level performance optimization and algorithm-level robustness enhancement, it is expected to jointly provide more flexible and efficient solutions for actual power systems.

Author Contributions: Z.H.: Investigation, Writing—review and editing, Methodology, Supervision. C.W.: Data curation, Methodology, Software, Writing—original draft. Y.G.: Conceptualization, Paper administration, Methodology, Supervision. H.Z.: Writing—review and editing, Methodology, Supervision. Z.L.: Writing—review and editing, Methodology, Supervision. P.W.: Writing—review and editing, Methodology, Supervision. All authors have read and agreed to the published version of the manuscript.

Funding: This research received no external funding.

Data Availability Statement: The data presented in this study are available on request from the corresponding author.

Acknowledgments: This work was supported in part by the National Natural Science Foundation of China under Grant 52467004, in part by the Key Research and Development Program of Jiangxi Province under Grant 20261BCE310047, and in part by the international exchange project from Department of Science and Technology of Jiangxi Province under Grant 20242BCE50086.

Conflicts of Interest: The authors declare no conflicts of interest.

References

1. Roboam, X. A Review of Powertrain Electrification for Greener Aircraft. *Energies* **2023**, *16*, 6831. [CrossRef]
2. Setlak, L.; Kowalik, R.; Gębura, A.; Gołda, P. Dynamic stability analysis of the aircraft electrical power system in the more electric aircraft concept. *Sci. Rep.* **2024**, *14*, 25521. [CrossRef] [PubMed]
3. Barzkar, A.; Ghassemi, M. Components of Electrical Power Systems in More and All-Electric Aircraft: A Review. *IEEE Trans. Transp. Electrif.* **2022**, *8*, 4037–4053. [CrossRef]
4. Zhang, J.; Roumeliotis, I.; Zolotas, A. Sustainable Aviation Electrification: A Comprehensive Review of Electric Propulsion System Architectures, Energy Management, and Control. *Sustainability* **2022**, *14*, 5880. [CrossRef]
5. Lei, T.; Min, Z.; Gao, Q.; Song, L.; Zhang, X.; Zhang, X. The Architecture Optimization and Energy Management Technology of Aircraft Power Systems: A Review and Future Trends. *Energies* **2022**, *15*, 4109. [CrossRef]
6. Gao, Y.; Yang, T.; Bozhko, S.; Wheeler, P.; Dragicevic, T.; Gerada, C. Neural Network aided PMSM multi-objective design and optimization for more-electric aircraft applications. *Chin. J. Aeronaut.* **2022**, *35*, 233–246. [CrossRef]
7. Dorn-Gomba, L.; Ramoul, J.; Reimers, J.; Emadi, A. Power Electronic Converters in Electric Aircraft: Current Status, Challenges, and Emerging Technologies. *IEEE Trans. Transp. Electrif.* **2020**, *6*, 1648–1664. [CrossRef]
8. Zhao, Y.; Huang, W.; Bu, F. Direct Power Control of a Bipolar Output Active Rectifier for More Electric Aircraft Based on an Optimized Sector Division. *World Electr. Veh. J.* **2023**, *14*, 89. [CrossRef]
9. Wang, C.; Yang, T.; Lang, X.; Bozhko, S. An Advanced Switching Harmonic Cancellation Method for a Dual-Generator Power System in More-Electric Aircraft. *IEEE J. Emerg. Sel. Top. Power Electron.* **2022**, *10*, 7120–7132. [CrossRef]

10. Poon, J.; Johnson, B.; Dhople, S.V.; Rivas-Davila, J. Decentralized Carrier Phase Shifting for Optimal Harmonic Minimization in Asymmetric Parallel-Connected Inverters. *IEEE Trans. Power Electron.* **2021**, *36*, 5915–5925. [CrossRef]
11. Huang, Z.; Xiao, X.; Gao, Y.; Ji, B. Harmonic Cancellation for Dual-Generator Power Systems in More-Electric Aircraft: A Neural Network Approach. In *Proceedings of the 2024 IEEE International Conference on Electrical Systems for Aircraft, Railway, Ship Propulsion and Road Vehicles & International Transportation Electrification Conference (ESARS-ITEC), Naples, Italy, 26–29 November 2024*; IEEE: New York, NY, USA, 2024; pp. 1–6. [CrossRef]
12. Huang, Q.; Li, Y.; Dou, Y.; Li, Y.; Zhu, J.; Li, S. History-Dependent Prandtl–Ishlinskii Neural Network for Quasi-Static Core Loss Prediction Under Arbitrary Excitation Waveforms. *IEEE Trans. Power Electron.* **2025**, *40*, 9625–9637. [CrossRef]
13. Zhao, C.; Zuo, Y.; Wang, H.; Lee, C.H.T. Online-Trained Radial Basis Function Neural Network Compensator for Current Harmonics Suppression of Electric Drives. *IEEE Trans. Ind. Electron.* **2024**, *71*, 15488–15498. [CrossRef]
14. Xiao, L.; Sattarov, R.R.; Liu, P.; Lin, C. Intelligent Fault-Tolerant Control for AC/DC Hybrid Power System of More Electric Aircraft. *Aerospace* **2022**, *9*, 4. [CrossRef]
15. Wang, S.; Yang, Z.; Zhang, Q. A Neural Network-Based Fault-Tolerant Control Method for Current Sensor Failures in Permanent Magnet Synchronous Motors for Electric Aircraft. *Aerospace* **2025**, *12*, 697. [CrossRef]
16. Zhu, Z.; Lin, K.; Jain, A.K.; Zhou, J. Transfer Learning in Deep Reinforcement Learning: A Survey. *IEEE Trans. Pattern Anal. Mach. Intell.* **2023**, *45*, 13344–13362. [CrossRef] [PubMed]
17. Chen, H.; Luo, H.; Huang, B.; Jiang, B.; Kaynak, O. Transfer Learning-Motivated Intelligent Fault Diagnosis Designs: A Survey, Insights, and Perspectives. *IEEE Trans. Neural Netw. Learn. Syst.* **2023**, *35*, 2969–2983. [CrossRef] [PubMed]
18. Won, Y.J.; Kim, J.-H.; Park, S.-H.; Lee, J.-H.; An, S.-M.; Kim, D.-Y.; Lim, M.-S. Transfer Learning-Based Design Method for Cogging Torque Reduction in PMSM with Step-Skew Considering 3-D Leakage Flux. *IEEE Trans. Magn.* **2023**, *59*, 8204905. [CrossRef]
19. Wang, Y.; Liu, R.; Lin, D.; Chen, D.; Li, P.; Hu, Q.; Chen, C.L.P. Coarse-to-Fine: Progressive Knowledge Transfer-Based Multitask Convolutional Neural Network for Intelligent Large-Scale Fault Diagnosis. *IEEE Trans. Neural Netw. Learn Syst.* **2023**, *34*, 761–774. [CrossRef] [PubMed]
20. Sapkota, D.B.; Neupane, P.; Pokharel, K.; Khan, S. An Artificial Neural Network Based Approach for Harmonic Component Prediction in a Distribution Line. *Energy Rep.* **2024**, *12*, 3861–3873. [CrossRef]
21. Lang, X.; Yang, T.; Huang, Z.; Wang, C.; Wang, Z.; Bozhko, S.; Wheeler, P. Stability Improvement of Onboard HVdc Grid and Engine Using an Advanced Power Generation Center for the More-Electric Aircraft. *IEEE Trans. Transp. Electrif.* **2022**, *8*, 660–674. [CrossRef]
22. Wang, Q.; Fu, H.; Chen, Z.; An, B.; Ma, Z. Fixed-time reinforcement learning fault-tolerant control for uncertain nonlinear systems with actuator saturation and time-varying bias faults. *Eng. Appl. Artif. Intell.* **2026**, *170*, 114250. [CrossRef]

Disclaimer/Publisher's Note: The statements, opinions and data contained in all publications are solely those of the individual author(s) and contributor(s) and not of MDPI and/or the editor(s). MDPI and/or the editor(s) disclaim responsibility for any injury to people or property resulting from any ideas, methods, instructions or products referred to in the content.